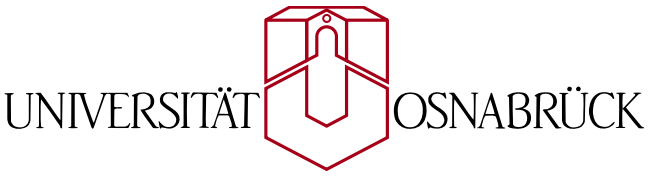

Department of Computer Science
Department of Cognitive Science

Rasmus Diederichsen

Designing And Implementing A Rephotography Application For iOS

Bachelor's Thesis

First Supervisor: Prof. Dr. Oliver Vornberger
Second Supervisor: Dr. Thomas Wiemann

CONTENTS

LIST OF TABLES

LIST OF FIGURES

1 INTRODUCTION

This chapter will introduce the notion of rephotography, elaborate on the process of how to make such a photograph and survey existing approaches to simplify it. These include two applications for mobile operating systems which will be briefly discussed. Furthermore, a summary of more sophisticated work by MIT researchers will be given, leading to the problem statement and the goal of this work.

1.1 OVERVIEW

Rephotography or repeat photography denotes the retrieval of the precise viewpoint used for taking a—possibly historic—photograph and capturing another image from the same spot, ideally with the same camera parameters. This allows for documentation and visualisation of changes which the scene has undergone between the two or more captures. For instance when documenting urban development, one can present progress of construction, restoration efforts or changes in the surroundings in a visually striking manner, e.g. by blending the photographs together. Figures 1.1 and 1.2 show examples.

When done manually, the photographer must attempt to find the original viewpoint usually by visual inspection of the original image and trying to match the current camera parameters—camera position, camera rotation, focal length, possibly principal point—to the original. The procedure is often carried out by placing the camera on a tripod and comparing a printout of the original image with what can be seen through the viewfinder or the camera screen. The number of parameters to match as well as the difficulty to estimate them purely from comparing two-dimensional images makes the process error-prone and tedious. Visual acuity and experience of the photographer thus place limits on the accuracy with which the camera pose of the reference image can be reconstructed. Some corrections can be done by post-processing the images and warping the rephotograph with a homography to better match the original.

At the time of writing, few computerised aids are available to the photographer (see below). The advancement of mobile phones and tablet computers with integrated cameras and larger screens presents the opportunity to develop applications which can assist in this endeavour, moving away from the traditional trial-and-error approach. On current digital cameras[1] this is impossible due to their closed infrastructure not permitting running user programs.

1 At the time of writing, no commercial manufacturer produces a camera with user-modifiable firm- or software. A project at Stanford (Adams et al., 2010) was discontinued Levoy (2009)

Figure 1.1: Residenzschloss Dresden, destroyed during World War II, © Sergey Larenkov, printed with permission

Figure 1.2: Frauenkirche Dresden, destroyed during World War II, © Sergey Larenkov, printed with permission

1.2 PREVIOUS APPROACHES

1.2.1 *Mobile Applications*

Two applications have been developed to assist a photographer in taking rephotographs. For smartphone operating systems, *rePhoto*[2] and *Timera*[3] exist, both available for Android and iOS devices. These applications support the user by placing a transparent version of the original image over the current camera image, allowing for easier alignment. The captured rephotograph is then presented together with the original image in a blend (c.f. **??**) which can be customized in *Timera*.

What is characteristical about both of these applications is that the user must still determine on their own how to actually move the camera. An overlay simplifies the procedure, eliminating some of the inaccuracy introduced into the manual approach by the necessity to move the eyes from printout to camera, but it is still the user's responsibility to determine the necessary motion between the current camera position and the goal position (that of the original image).

1.2.2 *Computational Re-Photography*

A more sophisticated automated approach was presented in by MIT researchers in 2010. Bae et al. (2010) found in preliminary studies that neither a side-by-side view as would be used in the manual approach, nor a linear blend provided by the above applications result in accurate rephotographs.

In this setup, the relevant parameters of a historic image's camera are reconstructed, including the focal length, principal point and the six degrees of freedom in camera pose. This subsection will give a high-level overview, while a more in-depth discussion of the relevant concepts is deferred until **??**.

The software runs on a laptop connetcted to a digital camera. After reconstructing the scene in 3D by use of two images captured by the user, they are then directed by the software to the desired viewpoint, the user does not have to find it by themselves. On the screen, they are shown the current camera image alongside two arrows indicating in which direction to move—one for movement in the sensor plane and one for movement along the optical axis.

Bae et al. (2010) identify five primary obstacles in viewpoint reconstruction of a historic photograph.

1. The necessary camera motion has six degrees of freedom—three for translation and three for rotation—which are challenging for the user to adjust simultaneously, as changing one parameter will often necessitate adjustments for the others to improve the matching. Furthermore, the number of degrees of freedom

2 http://projectrephoto.com/
3 http://www.timera.com/Explore

makes it difficult to communicate to the user how they must move the camera.

2. Computing relative translation between two cameras from corresponding image points is possible only up to an unknown scale (see **??**), meaning it is impossible to determine e.g. if an object viewed by the camera is small and close or large and further away. This poses the problem of how to determine if the user is close to the desired viewpoint and whether or not they have come closer or moved further away over iterations.

3. Relative pose estimation from corresponding points fails when the motion between the two cameras approaches zero, which is the ultimate goal one wishes to achieve. When naïvley comparing the current camera image to the reference photograph, the estimate for relative rotation and translation would become increasingly unreliable as the camera approaches the original viewpoint.

4. Automated computation of relative camera pose will rely on feature detection to find correspondences. However, historical images will often be vastly different from the current scene. Not only may the scene itself have changed considerably, but also the historical image—having been taken by a historical camera—may differ in contrast, sharpness and colours. Feature detectors may not be able to reliably find correspondences when comparing an old with a new photograph.

5. The calibration data—most importantly, focal length and principal point—of the historical camera are often unknown. The calibration data is needed for relative pose computation.

Initially, after loading a historical image, the user is instructed to take two photographs of the scene with a reasonably wide baseline (about 20°). One of them, termed *first frame* is supposed to be taken from some distance from the original viewpoint, the *second frame* should be the user's best eyeballed approximation of it. The wide baseline allows for a more reliable 3D-reconstrution of the scene used to tackle problems 2. and 3.

SIFT features (Lowe, 1999) are computed and matched between the two images. Given these correspondences, 3D coordinates of the points can be computed. A selection of these is reprojected into the second frame after which the user identifies six or more points in the historical photograph corresponding to these points in the second frame. This allows estimating extrinsic and intrinsic camera parameters of the historical camera by running an optimisation algorithm on an initial estimate for relative rotation and translation between first frame and reference image as well as sensor skew, focal length and principal point of the historical camera (problem 5.). The principal point's initial guess is found again with help of the user who identifies three sets of parallel lines in the historical image (see Hartley and Zisserman, 2004, chapter 8.8).

The result is that the location of the reference camera relative to the first camera is known. During the homing process, the current camera frame is compared to the first frame (not the reference frame, avoiding problem 3.), which avoids degeneracy due to the wide baseline. Given the locations of the reference camera and the current frame's camera, each relative to the first frame, one can compute the location of the reference relative to the current frame and thus guide the user in the right direction. Hence, the reference photograph is not needed anymore after this initial step, circumventing problem 4.

During homing, the current camera frame is warped according to the necessary rotation before being shown to the user, allowing them to focus only on the translation (problem 1.). This is possible since for rephotography dealing with structures usually at some distance, the rotation will be small, otherwise the warped image would be unusable.

A remaining problem (2.) is that the scale of the necessary translation is unknown, so that only the direction is known. This poses the question of how to determine whether the user has come closer to the goal or not. It may be feasible to find the original viewpoint nonetheless, if it was possible to determine at least when the user reaches it, but this is impossible without further information. On top of that, it would make for a better user experience if also the distance to the goal could be communicated.

A key observation in this regard is that the actual scale of the translation is irrelevant, it is sufficient that there be a way to make the scale consistent accross iterations. That is, it is unnecessary to know whether the goal is a specific distance aways, if one can ensure that the translations computed one after the other can be somehow meaningfully compared. For this, Bae et. al observe that when triangulating 3D coordinates from corresponding points, their computed distance from the camera (the first frame) is inversely proportional to the distance between the cameras. Therefore, in each iteration, the scale of the world is computed by triangulating correspondences between the first and current frames. The scale is compared to the scale computed in the initial step for the first and second frames. Scaling the current translation vector by the ratio of the two scales makes the length consistent across iterations and decreasing with the distance to the goal.

The results of this method appear to be very successful, but two main drawbacks exist.

- The prototype is not very convenient, as it requires a (laptop) computer and a digital camera to carry out which is impractical for spontaneous rephotography.
- The application is not available to the public, neither in source nor binary form. It is therefore impossible to evaluate adapt for more mobility.

1.3 GOALS OF THIS THESIS

This work's objective can thus be summarised as follows.

1. Implement in a prototypal fashion the process from (Bae et al., 2010) for a mobile operating system so it can be run on a smartphone or tablet and direct the user in approximate real-time.

2. Evaluate the approach and attempt to reproduce the results.

For a proof-of-concept application, several simplifying assumptions are made. Firstly, it is assumed that the "historic" photograph is captured with the same camera as the application is run on and that the camera is calibrated. Secondly, no strong visual differences between the reference and current scenes are assumed so that the reference image is accessible to the same feature detection algorithm without the user manually labelling correspondences.

The application targets iOS 8 and current hardware, as image processing is computationally intense, and has been tested on an iPad Air 2.

2

CAMERA GEOMETRY

This chapter will introduce the geometry of image projection, largely following (Hartley and Zisserman, 2004, chapters 6,7) and the geometry of two views (the epipolar geometry, Ma et al. (2003, ch. 5.1)) and how it can be used to recover relative camera position from two images of the same scene.

2.1 CAMERA MODELS

The camera model used is the ideal pinhole camera model which postulates several idealised assumptions.

1. The aperture size is infinitely small
2. There are no lens effects (*thin lens* assumption)
3. The angle of view is arbitrarily large
4. All world points projected onto the image plane are in focus, owing to the small aperture

Homogeneous vectors are the elements of projective geometry. They can be obtained from cartesian coordinates by appending a 1-element. All projective entities which differ only by a scalar factor are equivalent, one writes $\mathbf{x} \sim \mathbf{y}$ if $\mathbf{x} = \lambda\mathbf{y}, \lambda \neq 0$. This has the added effect that points at infinity can be represented by vectors whose last coordinate is zero.

Given a camera C whose center of projection is the origin and a point $\mathbf{X}$ in camera-centric coordinates, the central projection of $\mathbf{X}$ onto C's image plane is depicted in a side-view in Figure 2.1. The image plane is virtually moved to the front of the camera, otherwise the image would be mirrored at the principal point as in real cameras. Let f be the focal length, which is the distance of the image plane to the optical centre. If $\mathbf{X} = (X, Y, Z)$, then $x = \left(f\frac{X}{Z}, f\frac{Y}{Z}, f\right)$ by use of the intercept theorem.

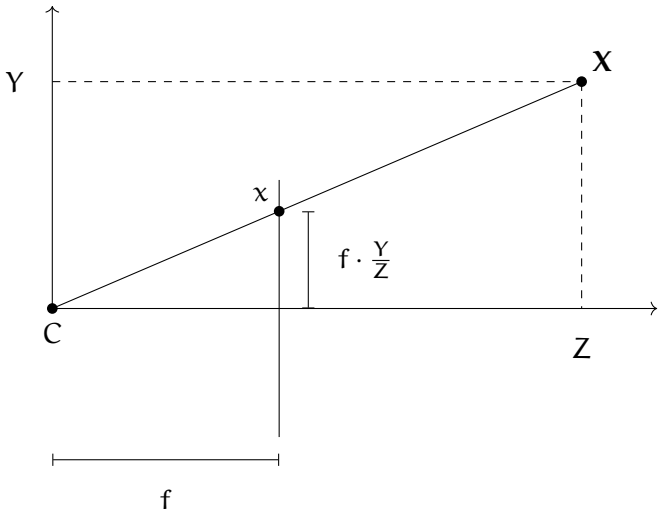

Figure 2.1: Central projection for a pinhole camera

When representing the points as homogeneous quantities, the central projection can be expressed by a matrix multiplication. This can be written with homogeneous coordinates as

$$\begin{pmatrix} fX \\ fY \\ Z \end{pmatrix} = \underbrace{\begin{pmatrix} f & 0 & 0 & 0 \\ 0 & f & 0 & 0 \\ 0 & 0 & 1 & 0 \end{pmatrix}}_{\text{Projection Matrix of C}} \begin{pmatrix} X \\ Y \\ Z \\ 1 \end{pmatrix} \tag{2.1}$$

or in short

$$\mathbf{x} \sim P\mathbf{X} \tag{2.2}$$

2.1.1 *Camera Extrinsics*

The above situation is a special case wherein the camera centre C defines the origin and the optical and image axes are the coordinate axes. Thus, the rotation and translation of the camera relative to this coordinate system is zero. More generally, there might be a world coordinate frame with different origin and different axes, so that a coordinate transform must be applied to $\mathbf{X}$ before the projection.

Let $R \in \mathbb{R}^{3\times3}$ be a rotation matrix giving the camera's rotation relative to the world frame and $t \in \mathbb{R}^{3\times1}$ its translation such that

$$\mathbf{X}_{\text{cam}} = R\mathbf{X}_{\text{world}} + t \tag{2.3}$$

Then the projection of a point $\mathbf{X}$ in world coordinates onto the image plane becomes

$$\mathbf{x} = P\mathbf{X} \tag{2.4}$$

$$\mathbf{x} = \begin{pmatrix} f & 0 & 0 \\ 0 & f & 0 \\ 0 & 0 & 1 \end{pmatrix} [R \mid t]\,\mathbf{X} \tag{2.5}$$

2.1.2 *Camera Intrinsics*

Above, the resulting image points $\mathbf{x}$ were in *normalised* image coordinates. In particular, the principal point—the intersection of the image plane with the optical axis—was assumed to be $(0, 0)$. But generally, image coordinates are expressed in pixels relative to the upper left corner of the sensor. To convert between normalised and pixel coordinates, the camera's five intrinsic parameters and can be written in matrix form and premultiplied in equation (2.5) as

$$\mathbf{x} = \begin{pmatrix} s_x & s & c_x \\ 0 & s_y & c_y \\ 0 & & 1 \end{pmatrix} \begin{pmatrix} f & 0 & 0 \\ 0 & f & 0 \\ 0 & 0 & 1 \end{pmatrix} [R \mid t]\,\mathbf{X} \tag{2.6}$$

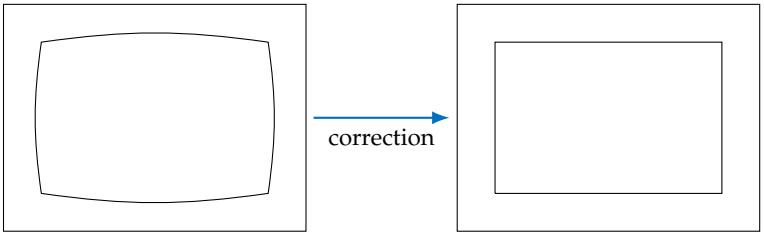

Figure 2.2: Radially distorted image on the left, the corrected image on the right.

where s_x and s_y are the focal lengths in x- and y-directions expressed in pixel units per world unit (e.g. cm; s_x and s_y are not necessarily identical, if the sensor has non-square pixels), s the sensor skew (the pixels may not be rectangular; their edges may not be perpendicular) which is usually zero, and the coordinates of the principal point (c_x, c_y) with respect to the origin of the image plane which usually placed at the upper left corner. The intrinsic camera parameters are assembled in

$$K = \begin{pmatrix} fs_x & s & c_x \\ 0 & fs_y & c_y \\ 0 & 0 & 1 \end{pmatrix} \tag{2.7}$$

are therefore essential to relate world points to image points which will be important for this application. The normalised coordinates $\hat{\mathbf{x}}$ for a pixel coordinate $\mathbf{x}$ can be computed as

$$\hat{\mathbf{x}} = K^{-1}\mathbf{x}, \tag{2.8}$$

which will remove the effects of the calibration parameters and thus make the image coordinates independent of the camera's internal characteristics.

In theory, these parameters could be obtained from the camera's vendor who knows the precise manufacturing specifications. In practice, only the focal lengths f_x, f_y are known, in most cases only one with the assumption of square pixels. Usually, the principal point is assumed to be at the sensor centre and the pixels are assumed to be rectangular. In practice however, there are variances introduced by different causes such as imprecise manufacturing or physical impacts which may decentre the lens such that the principal point is no longer at the centre.

A further compilcation is introduced by the camera lens which will often have a non-negligible distortion, most prominently radial distorion as depicted in Figure 2.2. It can be modeled by the application of a distortion factor to the ideal undistorted image coordinates $(\tilde{x}, \tilde{y})$.

$$\begin{pmatrix} x_d \\ y_d \end{pmatrix} = L(r) \begin{pmatrix} \tilde{x} \\ \tilde{y} \end{pmatrix} \tag{2.9}$$

where L is a nonlinear function of the distance r from the distortion center—usually coincident with the principal point. The function can be approximated as an exponential with a Taylor expansion

$$L(r) = 1 + \sum_{i=1}^{k} \kappa_i r^i \tag{2.10}$$

for a given k (see Hartley and Zisserman, 2004, ch. 7.4). The intrinsic camera parameters which consist in the entries of K and distortion coefficients κ_i must be determined in order to accurately relate world coordinates to image coordinates. They can be found by calibrating the camera. Different methods exist (e.g Zhang, 2000) but will not be examined here.

2.2 EPIPOLAR GEOMETRY

Epipolar geometry is the geometry which relates the image points in two views of the same scene. Figure 2.3 shows the basic setup.

We consider a scene viewed by two cameras with optical centres c_1 and c_2, where c_1 defines the origin, world points $\mathbf{X}_i \in \mathbb{R}^3$, where the subscript denotes the coordinate frame—the first camera, arbitrarily chosen to be the left one, or the second camera—and homogeneous image points $\mathbf{x}_i$ which are the projections of $\mathbf{X}_i$ onto the image planes and thus correspond to the same world point. The cameras are related by a rigid body transform (R, T), where R is a 3×3 rotation matrix and T the translation between the camera centres. Throughout this work, the direction of coordinate frame transformation will be such that

$$\mathbf{X}_2 = R\mathbf{X}_1 + T. \tag{2.11}$$

It is obvious that the following relation holds,

$$\lambda_i \mathbf{x}_i = \mathbf{X}_i, \ \lambda_i > 0 \tag{2.12}$$

that is, the world point lies on a ray through the optical centre and the image point.

Given the corresponding points $\mathbf{x}_i$ in two images, the ultimate goal is to retrieve the euclidean transform (R, T).

In case the image coordinates for both cameras are normalised (c.f. subsection 2.1.2), they have equal units, so starting from equation (2.11), one can derive

$$\begin{aligned}
\mathbf{X}_2 &= R\mathbf{X}_1 + T && \\
\lambda_2 \mathbf{x}_2 &= R\lambda_1 \mathbf{x}_1 + T && \text{(by equation (2.12))} \\
\lambda_2 \widehat{T}\mathbf{x}_2 &= \widehat{T}R\lambda_1 \mathbf{x}_1 + \widehat{T}T && \widehat{T} \in \mathbb{R}^{3\times 3} \text{ with } \widehat{T}\mathbf{x} = T \times \mathbf{x} \\
\lambda_2 \mathbf{x}_2^T \widehat{T}\mathbf{x}_2 &= \mathbf{x}_2^T \widehat{T}R\lambda_1 \mathbf{x}_1 + 0 && T \times T = 0 \\
\lambda_2 \cdot 0 &= \mathbf{x}_2^T \widehat{T}R\lambda_1 \mathbf{x}_1 && \widehat{T}\mathbf{x}_2 \text{ is perpendicular to } \mathbf{x}_2 \\
0 &= \mathbf{x}_2^T \underbrace{\widehat{T}R}_{E} \mathbf{x}_1 &&
\end{aligned} \tag{2.13}$$

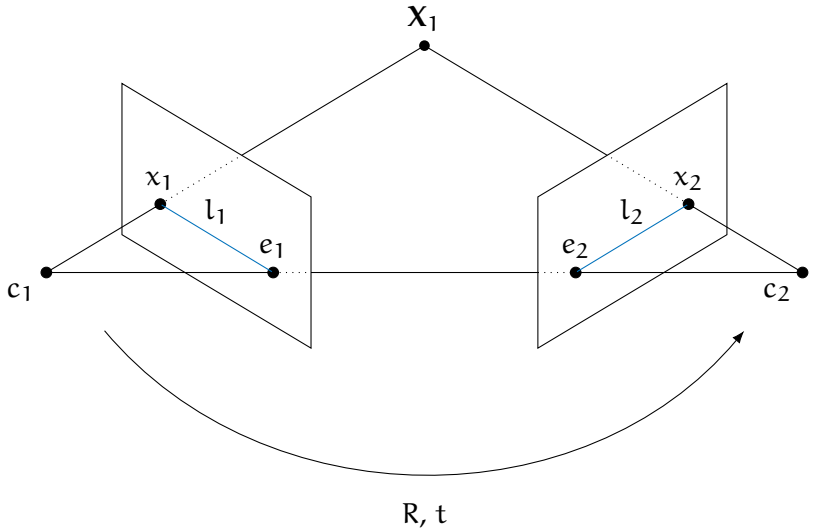

Figure 2.3: Basic epipolar geometry with camera centres c_1, c_2, image points $\mathbf{x}_1$, $\mathbf{x}_2$, a world point $\mathbf{X}_1$, epipoles e_1, e_2 and epipolar lines l_1, l_2

The product $E = \widehat{T}R$ is the *essential matrix* and the constraint it imposes on corresponding image points the *essential constraint* (see Ma et al., 2003, ch. 5).

An intuition for the essential matrix can be obtained from Figure 2.3. Given an image point in one frame $\mathbf{x}_1$, in attempting to find the point $\mathbf{x}_2$ corresponding to the same world point $\mathbf{X}_1$, the epipolar geometry restricts the search space to one dimension—the epipolar line of $\mathbf{x}_1$ in the second camera's image plane. The camera centres and the world point define an epipolar plane. The backprojection of $\mathbf{x}_1$ is the ray through $\mathbf{x}_1$ and the optical centre c_1. All points on this ray are mapped to the same point on the image plane of c_2. Depending on how far away the world point $\mathbf{X}_1$ is from c_1, its image on the second camera's image plane will vary—but it will be on the intersection of the image plane and the epipolar plane, the epipolar line of $\mathbf{x}_1$. The line l_2 may be identified with its coimage (the orthogonal complement of its preimage) $l_2 = e_2 \times \mathbf{x}_2 \in \mathbb{R}^3$ so that

$$\forall \mathbf{x} : \mathbf{x} \in l_2 \Leftrightarrow \mathbf{x} \cdot l_2 = 0. \tag{2.14}$$

The coimage of the epipolar line is the vector perpendicular to the epipolar plane, so every vector in this plane will have an inner product of 0 with this vector. Constrained to vectors in the image planes, this means that all vectors on the epipolar line will have an inner product of 0 with this vector l_2. Referring back to equation (2.13), it can be seen that multiplication with E will yield a term $\mathbf{x}_2^T E = l_2$ which fulfils

$$\mathbf{x}_1 \cdot l_2 = 0, \tag{2.15}$$

which is precisely the relation stated in equation (2.14). The essential matrix thus maps an image point onto its epipolar line in the other image.

2.3 ESSENTIAL MATRIX ESTIMATION

Estimating the essential matrix between two cameras and decomposing it into relative rotation and translation is a necessity in the endeavour to communicate a necessary camera movement to the application's user. The most prominent algorithms in this regard are the 8-Point algorithm introduced in its original form by Longuet-Higgins (1987) and improved upon by Hartley (1997), and the 5-Point algorithm proposed by Nistér (2004). To illustrate the mathematical tractability of the problem, the former will be presented below.

2.3.1 *The 8-Point Algorithm*

The essential matrix has nine elements, but since all image coordinates are projective quantities, the set of all essential matrices differing by a constant factor is equivalent so that one degree of freedom is removed and at most eight remain. If one were to formulate constraints on the elements as a system of linear equations, eight of those should be sufficient to uniquely determine an essential matrix. An improvement suggested in (Hartley, 1997) is the preprocessing of the input data (the image coordinates) by translation and scaling. This improves the robustness of the algorithm, but will be omitted here.

For each point correspondence $\{\mathbf{x}_1 = (x_1^i, y_1^i, 1), \mathbf{x}_2 = (x_2^i, y_2^i, 1)\}$, one linear equation

$$\mathbf{x}_2^T E \mathbf{x}_1 = 0 \tag{2.16}$$

is generated, which can be rewritten as

$$\begin{aligned} 0 = {} & x_2^i x_1^i e_{11} + x_2^i y_1^i e_{12} + x_2^i e_{13} \\ & + y_2^i x_1^i e_{21} + y_2^i y_1^i e_{22} + y_2^i e_{23} \\ & + x_1^i e_{31} + y_1^i e_{32} + e_{33} \end{aligned} \tag{2.17}$$

Let $\mathbf{e}$ denote the vector of E's entries in row-major order, then

$$0 = \left(x_2^i x_1^i, x_2^i y_1^i, x_2^i, y_2^i x_1^i, y_2^i y_1^i, y_2^i, x_1^i, y_1^i, 1\right) \cdot \mathbf{e} \tag{2.18}$$

If n correspondences are given, they each contribute one row to

$$A\mathbf{e} = \begin{bmatrix} x_2^1 x_1^1 & x_2^1 y_1^1 & x_2^1 & y_2^1 x_1^1 & y_2^1 y_1^1 & y_2^1 & x_1^1 & y_1^1 & 1 \\ \vdots & & & & & & & & \vdots \\ x_2^n x_1^n & x_2^n y_1^n & x_2^n & y_2^n x_1^n & y_2^n y_1^n & y_2^n & x_1^n & y_1^n & 1 \end{bmatrix} \mathbf{e} = 0 \tag{2.19}$$

For eight noise-free point correspondences in non-degenerate general position, there is a unique solution (up to scale) besides the trivial zero, but in practice, one uses more correspondences and the system is overdetermined, so a least-squares-solution minimising $\|A\mathbf{e}\| = \sum_{ij} (A\mathbf{e})_{ij}^2$ is sought. The solution is unique up to scale, since all multiples of $\mathbf{e}$ will satisfy equation (2.19). One therefore introduces the constraint $\|\mathbf{e}\| = 1$ which also excludes a trivial zero solution.

This solution vector is the singular vector with the smallest singular value in the singular value decomposition of A or equivalently, the smallest eigenvector of $A^\mathsf{T}A$ (see Hartley, 1997).

2.3.2 *Further Algorithms*

The 8-Point Algorithm is mathematically straightforward and linear, but in practice it suffers from noise (see Luong et al., 1993) and in real applications approaches the robustness of other methods only in its normalised form from (Hartley, 1997) (not related to *normalised image coordinates*).

It has been noted above that E can have at most eight degrees of freedom. In reality, it has only five, as rotation and translation have three degrees of freedom each, and one is lost due to the indeterminable scale. In theory five constraints from five pairs of image points thus are sufficient for finding E. A solution was put forth by Nistér (2004), improved in (Stewénius et al., 2006). The algorithm is nonlinear and thus much less easily understood and implemented, involving computing the roots of a ten degree polynomial, and requires only five points, but can also be applied to more. It can be considered a state-of-the-art solution to the relative pose estimation problem; its performance in overdetermined cases in the presence of noise compares favourably to other direct methods requiring six (Pizarro et al., 2003), seven or eight points.

Many other methods exist. Some—like the algorithms described above—find a globally optimal solution in closed form—, while others employ heuristic methods to iteratively approach a local optimum. A review is given in (Zhang, 1998).

Direct methods such as the five-point or eight-point algorithms are frequently used in schemes like RANSAC, which make the estimation more robust to outliers (correspondences which are imprecise or incorrect). For a number of iterations, a hypothesis for E is computed on a minimal number of correspondences and then evauluated on the whole data set. If the inliers in the data far outweigh the outliers, it is probable that a noise-free subsample is selected. The best hypothesis is kept. The simplified algorithm is shown in algorithm 1 (c.f. Hartley and Zisserman, 2004, ch. 4.8) and requires an error measure for E.

2.4 DECOMPOSING THE ESSENTIAL MATRIX

One step remains to recover the relative camera pose from corresponding points. As per the derivation in section 2.2, the rotation and translation between the two cameras is encoded in E. Given an essential Matrix, Hartley and Zisserman (2004, ch. 9.6) show that there are four mathematically valid decompositions of E into R and T, corresponding to four distinct geometrical scenarios (see Hartley and Zisserman, 2004, ch. 9.6). Only one of the solutions will place a point $\mathbf{X}_2 = \mathsf{R}\mathbf{X}_1 + \mathsf{T}$ in front of both cameras, the others cannot be realised in practice. Triangulating one point from its corresponding

Data: n point correspondences
Result: a best-fitting essential matrix
Let $c_{best} \coloneqq 0$;
for $i \coloneqq 0$, $i < maxIter$ **do**
  Select randomly a minimal number of points to estimate E_i;
  Compute error measure for E_i on all n points;
  Let C_i be the set of point pairs whose error does not exceed ε;
  if $|C_i| > c_{best}$ **then**
    $c_{best} \coloneqq |C_i|$;
    $E_{best} \coloneqq E_i$;
  end
end
return E_{best}

Algorithm 1: Simplified RANSAC scheme for essential matrix estimation

image points in the two views will therefore reveal the one correct solution, with the translation scale unkown.

3

CHALLENGES IN RELATIVE POSE ESTIMATION

The success of recovery of relative pose mainly depends on two factors: The accuracy and correctness of image point correspondences and them not being in a degenerate configuration, so that they provide enough information about the scene.

This chapter will examine the preconditions and the feasibility of pose recovery in realistic conditions. Several problematic cases will be identified and described. Furthermore, an assessment of different feature detection algorithms for the purpose of this work will be given.

3.1 DEGENERATE CONFIGURATIONS

Degenerate configurations are those in which the data on which the essential matrix is estimated allows for more than one mathematically valid solution. Two different cases can be observed.

3.1.1 *Structure degeneracy*

Structure degeneracy is a configuration of points in the observed scene which do not provide enough information to wholly determine an essential matrix. The projection matrix $P \in \mathbb{R}^{3\times3}$ with

$$\mathbf{x} = P\mathbf{X}$$

has twelve elements but is a projective quantity, so all non-zero multiples of P are equivalent, wherefore it has only eleven degrees of freedom. A degenerate case is for instance when all points observed by the two cameras lie on the same plane (or worse, a subspace of even lower dimension). The images of a planar surface in two cameras as well as the planar surface itself and its image are related by a homography (see Hartley and Zisserman, 2004, ch. 13), which is a mapping between planes and has eight degrees of freedom (being a 3×3 matrix and a projective element), meaning that three degrees of freedom are undetermined (Torr et al., 1999). A set of coplanar points thus does not provide enough information to uniquely determine an epipolar geometry without further information.

However, not all algorithms are susceptible to this problem. While the 8-point algorithm alone cannot deal with this case, the five-point algorithm can and is generally more robust (Li and Hartley, 2006). While there are other approaches to work around such issues (e.g. an algorithm developed by Chum et al. (2005) or Decker et al. (2008)), in practice, a five-point algorithm in a RANSAC scheme works well and needs fewer iterations than an 8-point approach (Li and Hartley, 2006).

3.1.2 *Motion Degeneracy*

A second type of degeneracy occurs when the camera motion between two images has fewer degrees of freedom than the model to be estimated—the essential matrix. If the camera only translates or only rotates between images, the motion has maximally three degrees of freedom. As Decker et al. (2008) point out, an essential matrix estimated under such conditions could be consistent with all correct point matches, but also with some false ones due to the mismatch in degrees of freedom between data and model. In schemes like RANSAC, such an estimate will have a large consensus set—all inliers *plus* outliers—and so may lead to the termination of the algorithm, despite being inaccurate.

It is unlikely in rephotography that the observed scene will be completely planar, or that the user will move from the first frame in a motion which is pure rotation or translation, these degeneracies can be labelled edge cases and are not specifically handled in the application.

3.2 FINDING CORRESPONDENCES

There is a variety of automatic feature detection algorithms which differ in repeatability, robustness to noise, speed and invariance with respect to image characteristics such as scale, brightness, or rotation. Generally, a feature detector identifies potentially salient points in an image and computes a descriptor for these points in a way that the same point under different conditions will yield an ideally identical descriptor. When points of interest—usually called *keypoints*—are available in multiple images, their descriptors can be compared and the best match according to some metric can be selected for each keypoint. The matches found can then be used as corresponding points for relative pose estimation.

Classical state-of-the-art detectors include e.g. SIFT (Lowe, 1999), SURF (Bay et al., 2006) which both compute real-valued descriptors. A natural criterion for selecting the best matching keypoint for a given keypoint is the L_2-norm of the difference of their descriptors, which is a relatively expensive operation. While e.g. SURF improves performance over the computationally demanding SIFT detector, the speed of matching can still present a bottleneck in time-critical contexts.

3.2.1 *SIFT*

3.2.2 *AKAZE*

4

EVALUATION

The approach has been evaluated on two realistic datasets. The most important questions are whether the direction of the necessary translation is correctly identified and its scale decreasing with distance to the target. For both sets of images, the ground-truth translation between each image and the first frame has been measured with centimetre accuracy, while the ground-truth rotation has been estimated from manually labelled correspondence as it is difficult to measure without the proper instruments. Since for the case of noise-free correspondences in a non-degenerate configuration, relative pose estimation algorithms are mathematically correct, this has been deemed sufficiently accurate to evaluate the procedure. For each image pair, 19–27 correspondences have been labelled, of which the majority is used for pose recovery. For pose recovery, RANSAC is used in conjunction with the five-point solver, a point is considered an inlier for a given essential matrix if its distance to its epipolar line is no more than three pixels. These parameters lead to the majority of points being inliers of the pose recovery, the few outliers can be explained by imprecise labelling.

In both data sets, the translation was mostly in the horizontal direction and along the optical axis; the vertical translation is thus neglected. Similarly, rotation was applied mainly around the vertical axis.

In order to idealise the condition, the reference photograph has been used to fill the role of the second frame for world scale computation. In reality, since the reference location is unknown, the reference world scale is obtained from a position somewhat off.

In all plots s refers to the scale at which the relative pose is computed. Besides the full resolution, the images are scaled down by factor of 2 (both dimensions are halved, resulting in quarter size) and 4 (sixteenth size). The resolutions evaluated are thus 3264×2448, 1632×1224, and 816×612.

The following graphics illustrate three things

1. The difference between the computed necessary rotation and the actually necessary one

2. The difference in direction of the computed necessary translation and the actually necessary one

3. The correlation between the true ratio of distances obtained by measuring camera movement and the average distance ratio computed with first and second (or in this case reference) frames based on automatic feature matching, at three different scales

4.1 TRAIN STATION DATA SET

In this series, the camera was moved horizontally from the reference to the right while also coming closer to the building. A schematic bird's eye view of the captures is shown in Figure 4.1.

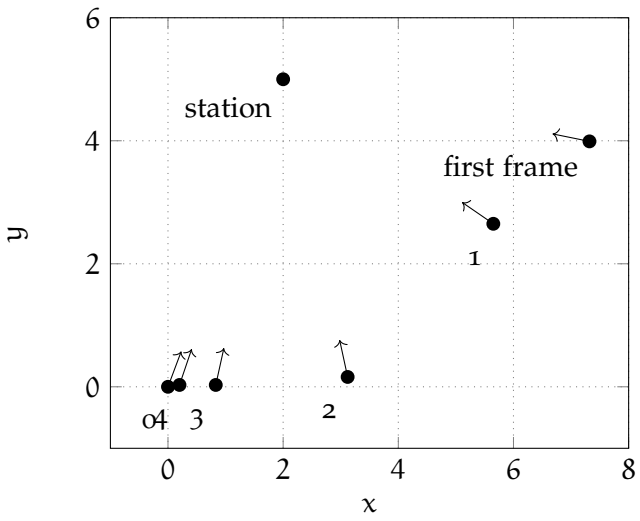

Figure 4.1: Schematic representation of the Train Station data set. Lengths and angles are not precise.

Table 1 summarises the ground truth for the five images.

4.1.1 *Scale Estimation*

Table 1: Ground truth for the train data. Image 0 is the reference frame, translations and rotations are given as in equation (2.11) relative to the reference frame.

Image number	Relative translation $[x, y, z]$	Relative Rotation $[\theta_x, \theta_y, \theta_z]$	ratio
0	$[0, 0, 0]$	$[0, 0, 0]$	1
1	$[.9053, 0, .4246]$	$[-3.3779, -9.3779, 1.05121]$	3.8936
2	$[.9986, 0, .0512]$	$[-1.3274, -5.7134, -.1884]$	1.6461
3	$[.9993, 0, .0361]$	$[-1.7156, -2.4761, .3469]$	1.0965
4	$[.9950, 0, .0995]$	$[.054606, -4.4867, .2452]$	1.0343

Figure 4.2 shows how the average distance of points to the first frame's camera varies with the second image used for triangulation. The plot illustrates that—especially at full resolution—the ratio based on feature matching closely mirrors the real value. The difference increases with decreasing image scale, but the slope of the graphs is quite similar. This shows that indeed with increasing distance to the first frame, the ratio decreases, allowing a deduction as to how close the camera is to the target, at least with respect to previous iterations, which is the primary objective. The decrease in ratio closely corre-

lates with the decrease in distance which is apparent on inspection of Figure 4.1. For instance, the viewpoints 3 and 4 are much closer together than e.g. 2 and 3, and the difference in ratios is much smaller between 3 and 4 as well.

The correlation is higher for AKAZE features than for SIFT ones, where a strong spike for image 1 can be observed. For SIFT, the decrease of ratio between images 2 and 3 is also hardly visible at $s = 2$. The unusual spike for image 1 poses the problem that the visualisation would tell the user that they need to move disproportionally far compared to the other images. Since the error in this case is corrected for the next image, this may not be a big problem, but will affect user experience. For SIFT features, one can also observe that the scale of the images appears to be less relevant, possibly an indication for the better scale invariance of the descriptor.

Generally, it can be concluded that on this data set, AKAZE features are an appropriate means of estimating the scale of relative camera translation.

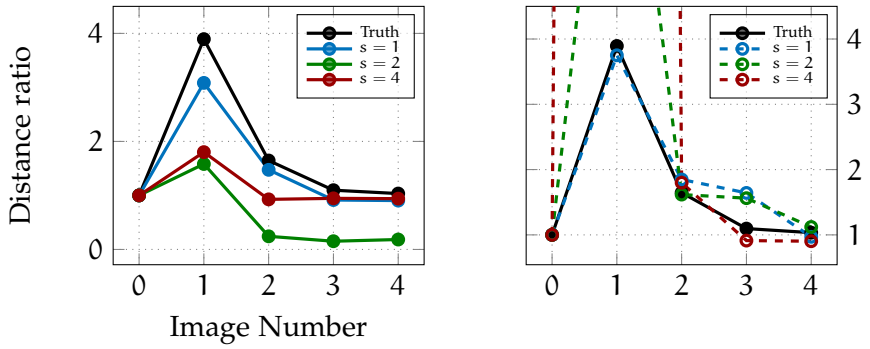

(a) AKAZE features (b) SIFT features

Figure 4.2: Train Station data set: Evolution of the distance ratio between images

4.1.2 *Rotation Estimation*

Figure 4.3 and Figure 4.4 illustrate the difference between the actually necessary camera rotation and the computed one for AKAZE and SIFT features, respectively. Rotations about the optical an X axes are small and thus not very interesting and the deviation is small.

Focusing on the Y-rotation, it is obvious is that the estimation quality decreases especially for $s = 4$, but the difference does not exceed 5 degrees and thus the estimate is very usable, especially since for reasonably quick updates, mostly the direction of necessary rotation is important, not the absolute magnitude.

The performance of SIFT is even better for scales $s = 1$ and $s = 2$, but slightly worse on the smallest scale (see Figure 4.4c).

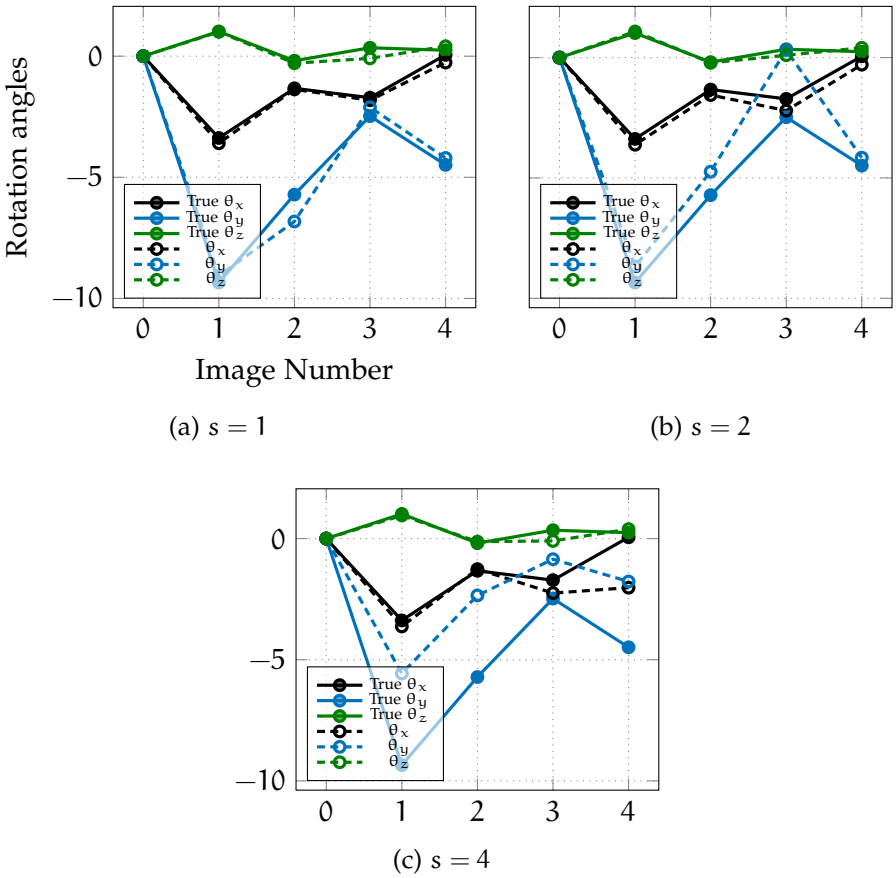

(a) s = 1

(b) s = 2

(c) s = 4

Figure 4.3: Train Station data set: Angles of rotation relative to reference with AKAZE features on full, quater and sixteenth resolution

4.1.3 *Translation Estimation*

Finally and most importantly, the directions of the necessary translation must be evaluated. Figure 4.5 plots the angular difference in degree between the actual necessary translation and the computed one. The reference frame 0 is omitted since the translation vector to compare with is $(0, 0, 0)$.

It is obvious that the estimates are completely useless, the difference exceeds 80 degrees in all cases. The results are so staggeringly bad as to be suggestive of conceptual or mathematical error, though none could be found. With these estimates, the user will be sent into an entirely wrong direction.

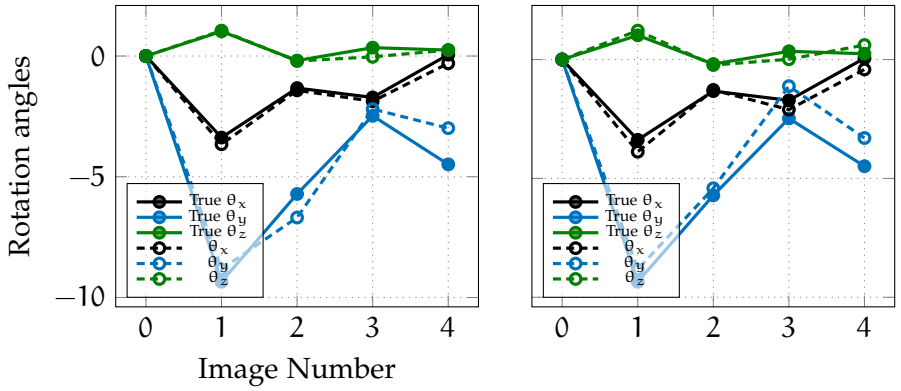

(a) s = 1 (b) s = 2

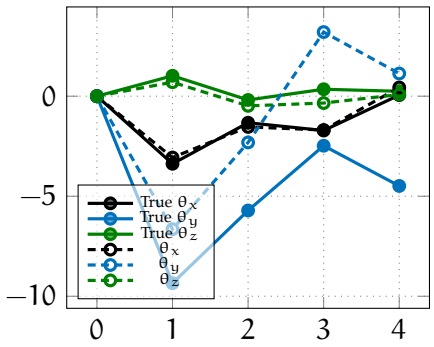

(c) s = 4

Figure 4.4: Train Station data set: Angles of rotation relative to reference with SIFT features

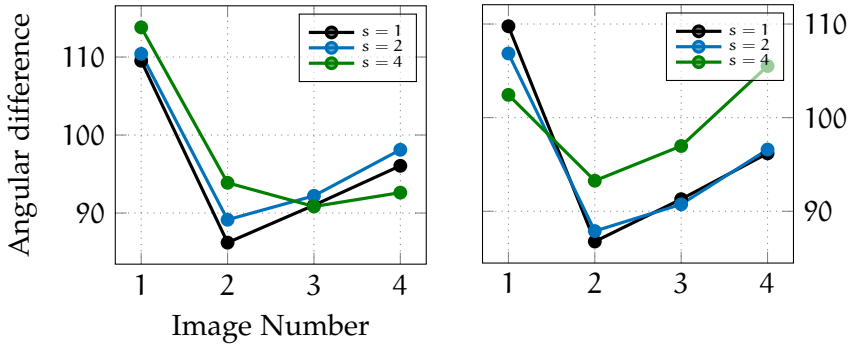

(a) AKAZE features (b) SIFT features

Figure 4.5: Train Station data set: Angular difference between actually necessary translation and algorithmic estimate

4.2 MANOR DATA SET

Seven images (including the reference photo) have been taken with movement to the right and backwards as well as forwards. The motif was always centred in the frame, thus there is prominent rotation around the y-Axis. The schematic positions for the seven manor captures (including reference photograph) are shown in Figure 4.6. In contrast to the train station set, there is more significant movement along the optical axis.

The ground truth data is summarised in Table 2.

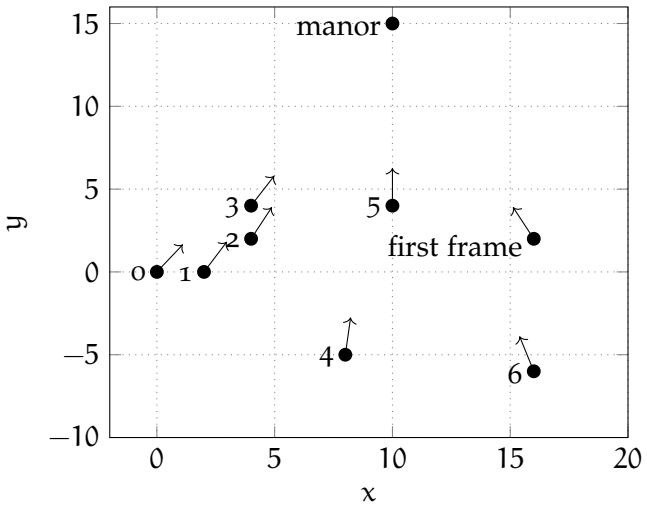

Figure 4.6: Schematic representation of the Manor data set. Lengths and angles are not precise.

Table 2: Ground truth for the manor data. Image 0 is the reference frame, translations and rotations are given as in equation (2.11) relative to the reference frame.

Image number	Relative translation $[x, y, z]$	Relative Rotation $[\theta_x, \theta_y, \theta_z]$	ratio
0	[0, 0, 0]	[0, 0, 0]	1
1	[1, 0, 0]	[−1.7857, −5.4827, 2.1073]	1.1401
2	[0.8944, 0., 0.4472]	[−2.1428, −6.5773, 1.6584]	1.3437
3	[0.7071, 0., 0.7071]	[0.7263, −5.0686, 2.6176]	1.3254
4	[0.8479, 0., −0.5299]	[−1.4146, −10.7998, 2.2250]	1.5168
5	[0.9284, 0., 0.3713]	[−0.1887, −16.6670, 1.2211]	2.5495
6	[0.9363, 0., −0.3511]	[−0.8725, −18.0933, 1.5385]	2.0155

4.2.1 *Scale Estimation*

The evolution of the translation scale is shown in Figure 4.7. It is apparent that the movement purely along the optical axis between images 2 and 3 is a problem. As the real distance to the target marginally

increases, so should the ratio, but it decreases instead. Frames 5 and 6 illustrate a problem with the scale estimation procedure itself. For it to work precisely, only movement along the line between first and reference frames is assumed, as a decreased distance to the first frame is interpreted as an increased distance to the reference frame, which is not necessarily the case as shown here. Even the "ground truth" computed from actual camera distances is thus of limited use.

For the AKAZE descriptor, only the full resolution comes reasonably close in magnitude and somewhat in slope. Wit SIFT, the slope is more accurately reproduced with $s = 2$, but strangely less accurately on full resolution. For the smallest scale, the estimate degenerates strongly.

Generally is can be stated that the estimates are less close than those for the train data set, but also that large movement along the optical axis shows the limits of this simple approach at scale estimation. Realistically, the user will not move as erratically so this kind of scenario is extreme.

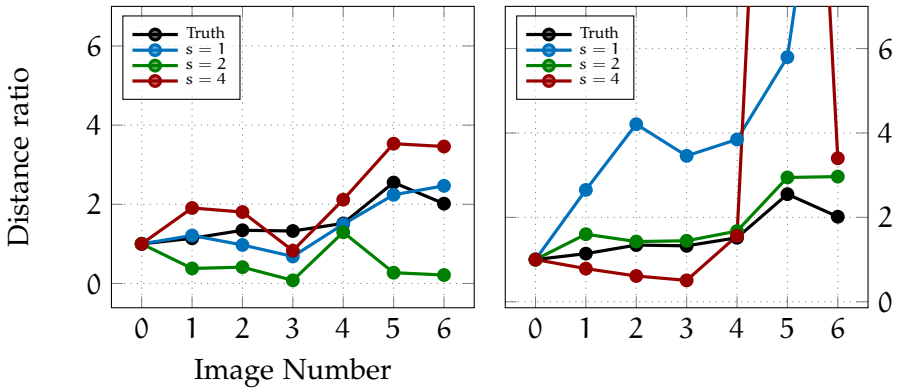

(a) AKAZE features (b) SIFT features

Figure 4.7: Manor data set: Evolution of the distance ratio between images

4.2.2 *Rotation Estimation*

Figure 4.8 and Figure 4.9 illustrate how accurately the necessary rotation is computed. On this data, AKAZE outperforms SIFT with default parameters (see **??**). On both full and half scale, there is negligible deviation from the truth, but on quarter scale, there are more than 5 degrees of difference and a complete failure for frame 3 (the direction is wrong, not only the magnitude).

With default parameters, SIFT compares much worse, particularly on full resolution where it grossly overestimates the necessary rotation. The results are better on the scaled-down images, possibly because of the reduction of noise, but still only partly useful on the smallest resolution.

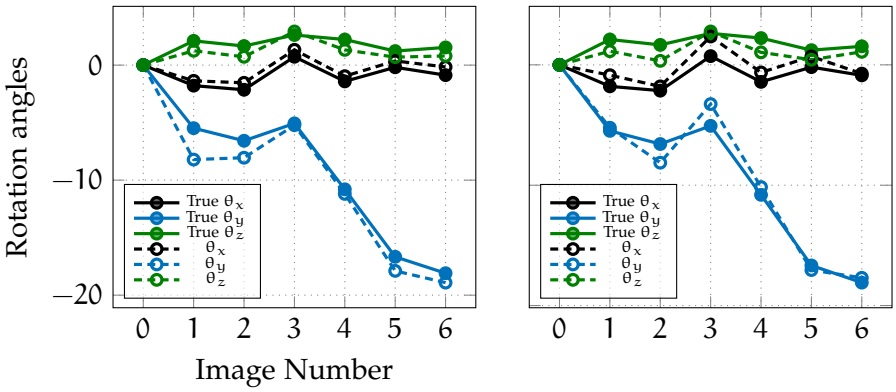

(a) s = 1

(b) s = 2

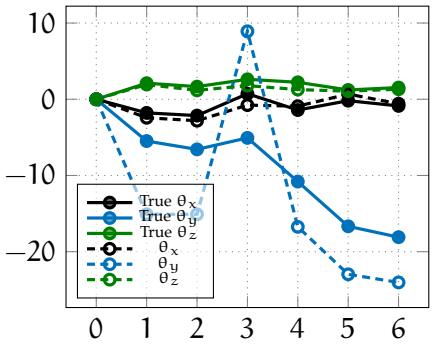

(c) s = 4

Figure 4.8: Manor data set: Angles of rotation relative to reference with AKAZE features

4.2.3 *Translation Estimation*

Lastly, the direction of necessary translation is evaluated in Figure 4.10. It is moot to discuss any improvement in comparison with the train data set, as the results are also completely false, SIFT displaying a larger variance than AKAZE, but neither are useful.

4.3 SUMMARY

Of the three pieces of information needed for user guidance, only the most important one—the direction of translation—cannot be recovered to any satisfying degree with this method. Both scale and necessary camera rotation estimation work, at least if the movement over iterations is mostly horizontal and not along the optical axis. A principal problem with the estimation of necessary translation could be observed. If the movement is mostly in one direction and the translation between reference and current frame is computed as

$$-R_{ref,first} R^{T}_{current,first} t_{current,first} + t_{ref,first}$$

then both summands will have mostly the same orientation which will consequently be zeroed out by the sign inversion of the first one. If the resulting vector is then normalised to unit length, the other two

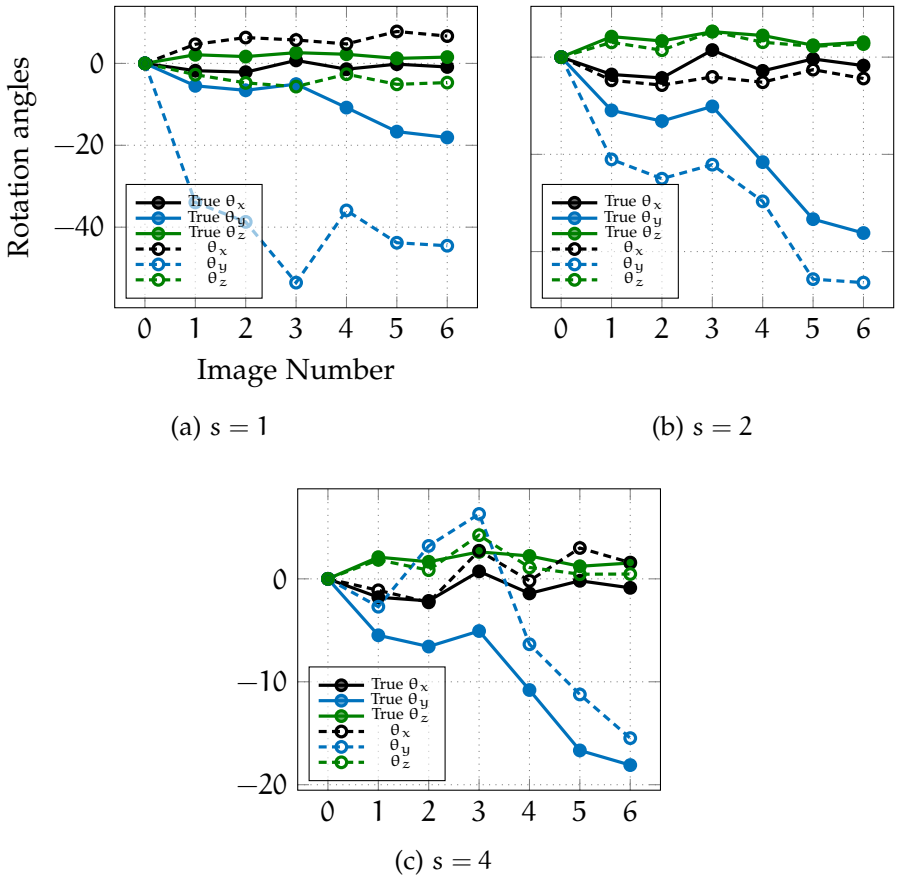

Figure 4.9: Manor data set: Angles of rotation relative to reference with SIFT features

dimensions will have nonzero values determined by small differences in their orientation and thus by noise and point into a completely wrong direction. Applying scale factors before the addition did not improve the situation. It is evident that this solution cannot work for movement in only on principal direction.

It could also be demonstrated that AKAZE features yield the more accurate results, except on the smallest scale, where SIFT compares somewhat favourably. The smallest scale however also leads to general deterioration in quality, suggesting that a scale between 2 and 4 may be required to combine accuracy with speed of processing.

Improvements for all estimates could possibly be improved by fine-tuning the parameters of both descriptors to adapt them to scenes with buildings, which has not been tried here.

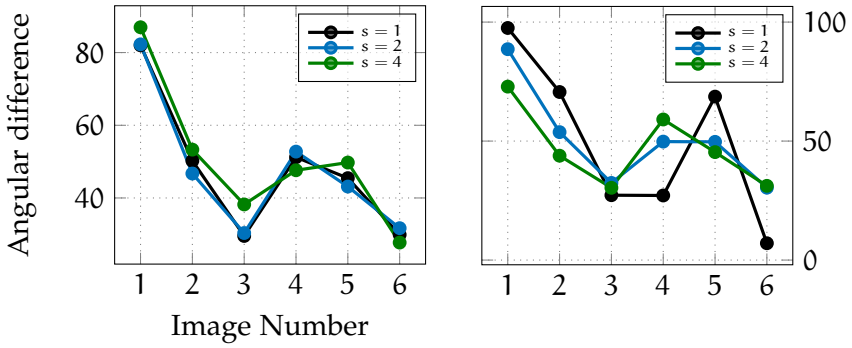

(a) AKAZE features (b) SIFT features

Figure 4.10: Manor data set: Angular difference between actually necessary translation and estimate

BIBLIOGRAPHY

Adams, A., Talvala, E.-V., Park, S. H., Jacobs, D. E., Ajdin, B., Gelfand, N., Dolson, J., Vaquero, D., Baek, J., Tico, M., Lensch, H. P. A., Matusik, W., Pulli, K., Horowitz, M., and Levoy, M. (2010). The frankencamera: An experimental platform for computational photography. *ACM Transaction on Graphics*, 29(4):29:1–29:12.

Bae, S., Durand, F., and Agarwala, A. (2010). Computational rephotography. *ACM Transactions on Graphics*, 29(3).

Bay, H., Tuytelaars, T., and Van Gool, L. (2006). Surf: Speeded up robust features. In *Computer vision–ECCV 2006*, pages 404–417. Springer.

Chum, O., Werner, T., and Matas, J. (2005). Two-view geometry estimation unaffected by a dominant plane. In *Computer Vision and Pattern Recognition, 2005. CVPR 2005. IEEE Computer Society Conference on*, volume 1, pages 772–779. IEEE.

Decker, P., Paulus, D., and Feldmann, T. (2008). Dealing with degeneracy in essential matrix estimation. In *Image Processing, 2008. ICIP 2008. 15th IEEE International Conference on*, pages 1964–1967. IEEE.

Hartley, R. I. (1997). In defense of the eight-point algorithm. *IEEE Transactions Pattern Analysis Machine Intelligence*, 19(6):580–593.

Hartley, R. I. and Zisserman, A. (2004). *Multiple View Geometry in Computer Vision*. Cambridge University Press, 2 edition.

Levoy, M. (2009). Camera 2.0: New computing platforms for computational photography. http://graphics.stanford.edu/projects/camera-2.0/. accessed 2015-07-28.

Li, H. and Hartley, R. (2006). Five-point motion estimation made easy. In *Proceedings of the 18th International Conference on Pattern Recognition - Volume 01*, ICPR '06, pages 630–633, Washington, DC, USA. IEEE Computer Society.

Longuet-Higgins, H. C. (1987). Readings in computer vision: Issues, problems, principles, and paradigms. chapter A Computer Algorithm for Reconstructing a Scene from Two Projections, pages 61–62. Morgan Kaufmann Publishers Inc., San Francisco, CA, USA.

Lowe, D. G. (1999). Object recognition from local scale-invariant features. In *Proceedings of the International Conference on Computer Vision-Volume 2 - Volume 2*, ICCV '99, pages 1150–, Washington, DC, USA. IEEE Computer Society.

Luong, Q.-T., Deriche, R., Faugeras, O., and Papadopoulo, T. (1993). On determining the fundamental matrix: analysis of different methods and experimental results. Research Report RR-1894.

Ma, Y., Soatto, S., Kosecka, J., and Sastry, S. S. (2003). *An Invitation to 3-D Vision: From Images to Geometric Models*. Springer Verlag.

Nistér, D. (2004). An efficient solution to the five-point relative pose problem. *IEEE Trans. Pattern Anal. Mach. Intell.*, 26(6):756–777.

Pizarro, O., Eustice, R., and Singh, H. (2003). Relative pose estimation for instrumented, calibrated imaging platforms. In *Proceedings of Digital Image Computing: Techniques and Applications*, pages 601–612, Sydney, Australia.

Stewénius, H., Engels, C., and Nistér, D. (2006). Recent developments on direct relative orientation. *ISPRS Journal of Photogrammetry and Remote Sensing*, 60:284–294.

Torr, P. H., Fitzgibbon, A. W., and Zisserman, A. (1999). The problem of degeneracy in structure and motion recovery from uncalibrated image sequences. *International Journal of Computer Vision*, 32(1):27–44.

Zhang, Z. (1998). Determining the epipolar geometry and its uncertainty: A review. *International Journal of Computer Vision*, 27(2):161–195.

Zhang, Z. (2000). A flexible new technique for camera calibration. *IEEE Transactions on Pattern Analysis and Machine Intelligence*, 22(11):1330–1334.